Estimation of Gyroscope Polhode Motion Using Trapped Magnetic Flux

C. E. Cohen, G. M. Keiser, B. W. Parkinson

Reprinted from

Journal of Guidance, Control, and Dynamics

Volume 15, Number 1, January–February 1992, Pages 152–158

AIAA

A publication of the
American Institute of Aeronautics and Astronautics, Inc.
The Aerospace Center, 370 L'Enfant Promenade, SW
Washington, DC 20024-2518

Estimation of Gyroscope Polhode Motion Using Trapped Magnetic Flux

Clark E. Cohen,* G. M. Keiser,† and Bradford W. Parkinson‡
Stanford University, Stanford, California 94305

A freely spinning body undergoes the well-known polhode motion of its spin axis. Applied to the cryogenic, electrostatically suspended spherical gyroscopes of the Gravity Probe B program, an unusual analysis technique is presented that allows reconstruction of the polhode motion, relying on the trapped magnetic flux in the superconducting rotor. Cooled to a temperature below 9 K, the niobium rotor coating becomes a superconductor, trapping the ambient magnetic field. Fixed with respect to the rotor body frame, this trapped magnetic flux is used as a reference against which to track the path of the rotor spin axis. The field is modeled as a series expansion in spherical harmonics. Consideration of any higher-order moment of the magnetic field along with the dipole moment is sufficient to completely define the spin axis coordinates in the body frame.

Introduction

Overview

LIKE the Earth, a superconducting gyroscope rotor possesses an intrinsic magnetic field. The key point is that this field rotates with the rotor. Through measurements of the magnetic field within the gyroscope housing, it is possible to build up an estimate of the field shape. Then, the field is used as a reference to reconstruct every aspect of the rotor motion, including the motion of the spin axis in the rotor body frame.

The problem consists of estimating simultaneously both the rotor motion and the magnetic field shape. Given knowledge of either the motion or the magnetic field by itself, one would expect that estimation of the other would be relatively straightforward. Simultaneous estimation of both unknowns, however, is more difficult.

A key feature of the estimation approach applied herein is that the higher-order components of the magnetic field shape are employed. No dynamic model is required. Simpler axially symmetric magnetic field models are not sufficient to completely define the orientation of the spin axis in the rotor body frame.

From this path, it is possible to calculate the rotor inertia difference ratios and infer the orientations of the rotor principal axes of inertia. Figure 1 depicts a set of polhodes based on a fit to experimental data. Once the magnetic field data can be referred to the principal axes of the rotor, this technique enables essential features of gyroscope physical properties to be quantified.

Gyroscope Specifics

Gravity Probe B is a space-based experiment being developed to measure two untested predictions of Einstein's General Theory of Relativity using orbiting gyroscopes.[1] The experiment goal is to measure the relativistic precession of the gyroscope spin axes with an accuracy of better than 1 milliarcsec over one year (3×10^{-11} deg/h). To assure that the drift rate due to Newtonian torques is less than 1 milliarcsec/year, the gyroscope rotor must be constructed with extreme care. Comprised of fused quartz, homogeneous in density ($\Delta\rho/\rho$) to less than 2×10^{-6}, the rotor is 3.82 cm in diameter, coated with a 2.5-μm layer of niobium. Three pairs of mutually orthogonal electrodes support the rotor electrostatically. The gyroscope is brought to its operating speed of 170 Hz with helium gas jets. Then, the housing is evacuated below 10^{-11} Torr for the experiment duration (nominally 18 months). Figure 2 is a photograph of a disassembled gyroscope and housing. Visible are four of the six circular suspension electrodes and the spin-up channel (at the center of the right housing). A thin film pick-up loop is deposited on the parting plane of the housing. The rotor must be spherical to within 20 nm (peak to valley), the rotor coating thickness uniformity must lie within 7.5 nm (peak to valley), and the inertia difference ratio $\Delta I/I$ must not exceed 10^{-6}.

Unlike most other gyroscopes, no attempt will be made to eliminate the natural polhode motion. Although components of the polhode motion will be measurable during the science mission, this motion is of greater importance in ground testing for ensuring the validity of experimental error models. Validation of the tracking technique described in this paper was performed using a rotor with $\Delta I/I$ of 10^{-4}.

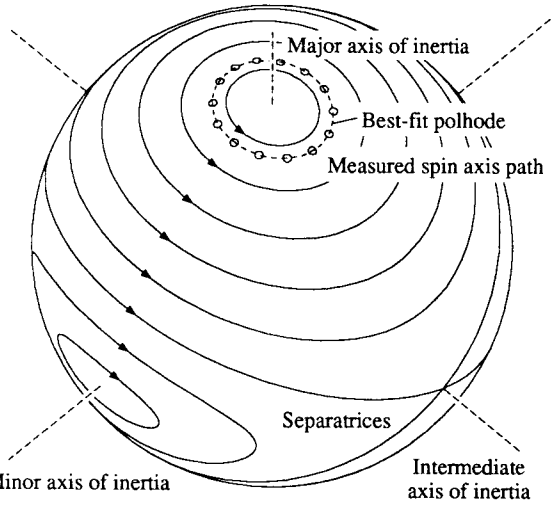

Fig. 1 Best-fit family of polhodes for Rotor 87R11c.

Presented as Paper 90-3419 at the AIAA Guidance, Navigation, and Control Conference, Portland, OR, Aug. 20-22, 1990; received Feb. 26, 1991; revision received July 15, 1991; accepted for publication July 15, 1991.

*Ph.D. Student, Department of Aeronautics and Astronautics, Gravity Probe B, MC 4085. Member AIAA.

†Senior Research Associate, W. W. Hansen Experimental Physics Laboratory, Gravity Probe B, MC 4085.

‡ Professor, Department of Aeronautics and Astronautics, Gravity Probe B, MC 4085; also Program Manager, Stanford Relativity Gyroscope Experiment. Fellow AIAA.

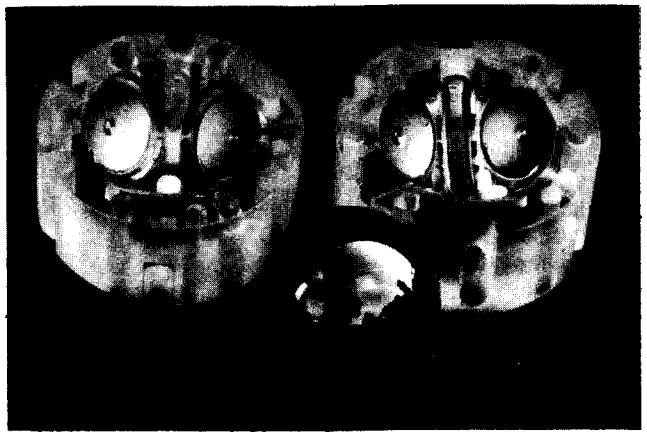

Fig. 2 Relativity gyroscope rotor and housing.

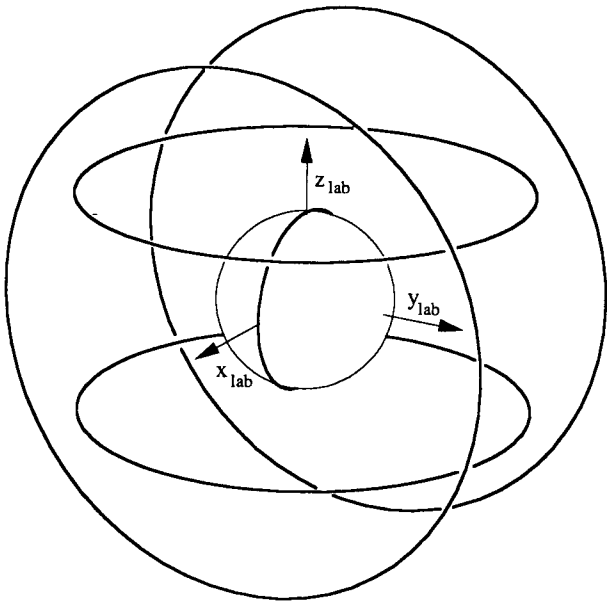

Fig. 3 Ground testing pick-up loop configuration.

Cooled below 9 K, the niobium gyroscope rotor coating superconducts. As the niobium transitions to the superconducting state, it traps the ambient magnetic field. Fixed with respect to the rotor body, the trapped flux serves as a reference against which to track the rotor spin axis motion.

The spin of the superconducting rotor also generates a magnetic moment parallel to the spin axis, which will be used to read out the direction of spin for the science mission. This field, called the London moment, has a strength of 10^{-4} G near the rotor surface for a 170-Hz spin rate. For the science mission, the London moment will dominate the trapped magnetic flux.

History of Trapped Flux Readout

Keiser and Cabrera[2] first applied trapped flux readout to estimating the polhode motion of a symmetric rotor with an inertia difference ratio $\Delta I/I$ of 10%. A dynamic model was assumed for the data analysis. Feteih et al.[3] modeled the trapped flux as a dipole, neglecting the higher-order shape of the magnetic field. Since the dipole moment is axially symmetric, its orientation with respect to the body frame provides only one of the two angular components necessary to fix the spin axis orientation.

Technique Description

This section briefly describes the hardware used for readout measurements then outlines the estimation scheme used to reconstruct the rotor motion.

Experimental Apparatus for Ground Testing

The magnetic field is measured in the laboratory reference frame by three orthogonal sets of superconducting wire pick-up loops in the configuration shown in Fig. 3. The two sets of outer pick-up loops are in a Helmholtz configuration, placed at radii of 3.36 and 2.86 of the rotor. The small, inner pick-up loop is nested inside the gyro housing separating plane at a radius of 1.025 of the rotor and is coupled inductively to a third Helmholtz pair. This inner loop is most sensitive to the higher-order detail in the magnetic field.

Superconducting quantum interference device (SQUID) magnetometers unobtrusively sense the pick-up loop flux as shown in Fig. 4. Figure 5 shows the experimental apparatus in the gyroscope ground test facility. The rotor, housing, and measurement pick-up loops are cooled by the dewar to 4.9 K. The field strength of the trapped flux near the rotor was ~9 mG for the polhode tracking experiments reported herein.

Data with rotor spin frequencies of order 10 Hz were analyzed. Each minute, the computer records a 5-s burst of 1024 samples (200 Hz). The samples are processed into Fourier amplitude and phase coefficients for each harmonic of the spin frequency. Based on calibration data, the amplitude and phase measurements are corrected for the transfer function of the apparatus. The resulting Fourier coefficients Φ_m yield the instantaneous spectrum (assuming that the spin axis is fixed with respect to both the laboratory and body reference frames) for each burst of the pick-up loop magnetic flux $\Phi_M(t)$, where

$$\Phi_M(t) = \Phi_0 + \sum_{m=1}^{\infty} (\Phi_m e^{im\omega t} + \Phi_m^* e^{-im\omega t}) \tag{1}$$

Since the measured flux is real, the complex Fourier coefficients are constrained by $\Phi_{-m} = \Phi_m^*$.

Trapped Flux Model

A magnetic field model is employed to find the rotor motion that best fits the observed Fourier coefficients Φ_m for each burst of data from the sets of pick-up loops. The field model is developed as follows.

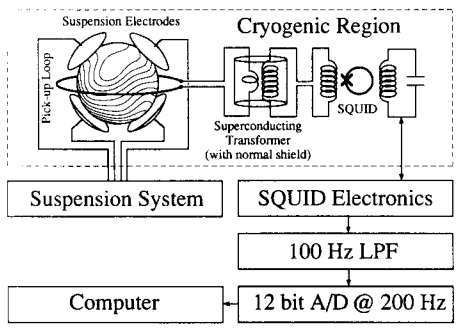

Fig. 4 SQUID magnetometer readout electronics.

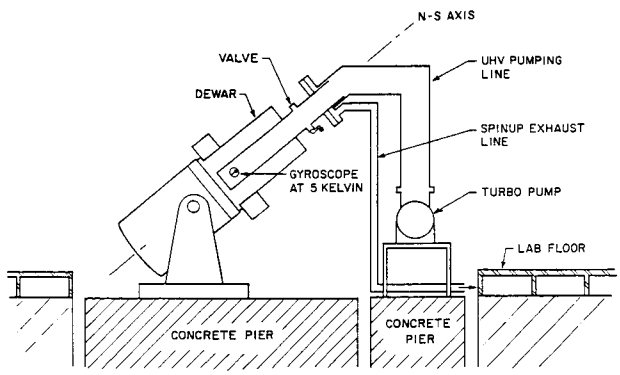

Fig. 5 Gyroscope ground test facility.

The magnetic field $\boldsymbol{B}(\boldsymbol{r})$ in the rotor-fixed frame may be expressed in terms of a scalar magnetic potential $V_M(\boldsymbol{r})$ such that $\boldsymbol{B}(\boldsymbol{r}) = -\nabla V_M$. In a region of space where there are no sources of magnetic fields, the scalar magnetic potential must satisfy Laplace's equation, $\nabla^2 V_M = 0$. Assuming that the scalar potential approaches zero at infinite radius, the most general solution to Laplace's equation in spherical coordinates is

$$V_M(\theta_R,\phi_R) = \sum_{l=1}^{\infty} \left(\frac{r_0}{r}\right)^{l+1} \sum_{m=-l}^{l} A_{lm} Y_{lm}(\theta_R,\phi_R) \qquad (2)$$

where the A_{lm} variables are complex model coefficients describing the magnetic field shape, r the radius of the point from the center of the rotor, r_0 the rotor radius, Y_{lm} the spherical harmonic basis function of order l and degree m, θ_R and ϕ_R the spherical coordinates defined in Fig. 6, and the subscript R denotes any rotor-fixed reference frame. Since the scalar potential is real, it must hold that

$$A_{l,-m} = (-1)^m A^*_{lm} \qquad (3)$$

The terms of order l comprise the lth-order magnetic moment of the trapped flux. The simplest moment is that of $l = 1$, the dipole, which may be expressed as a vector $\boldsymbol{T}$, related to the values of A_{10} and A_{11} by

$$A_{10} \sim \sqrt{2}\, T_z, \qquad A_{11} \sim -(T_x - iT_y) \qquad (4)$$

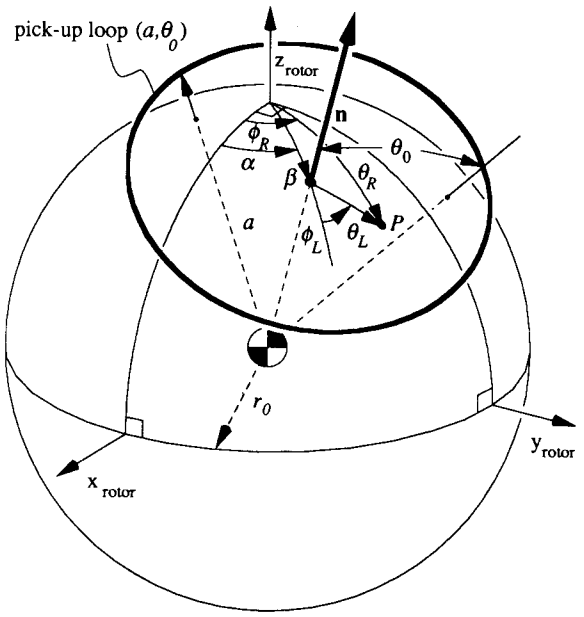

Fig. 6 Magnetic flux in the rotor reference frame.

As derived in the Appendix, the magnetic flux passing through a pick-up loop (shown in Fig. 6) may be calculated by integrating the radial component of the magnetic field over the spherical section enclosed by the loop. The resulting flux,

$$\Phi_M(\beta,\alpha) = r_0 \sum_{l=1}^{\infty} c_l\left(\frac{r_0}{a},\theta_0\right) \sum_{m=-l}^{l} A_{lm} Y_{lm}(\beta,\alpha) \qquad (5)$$

is a linear combination of each moment of the trapped flux at the normal to the pick-up loop (β,α). A topographical interpretation of this equation is depicted in Fig. 7 based on estimated values of the A_{lm} coefficients from experimental data. Each point on the left-most rotor contour map indicates the pick-up loop output when the loop normal passes through that point. This mapping can be expanded in spherical harmonics, comprised of magnetic moments of order l. Each moment of order l is comprised of the basis functions Y_{lm}. For reference, the spherical harmonic basis functions are shown for Y_{3m}, the third-order moment. Contours of the basis functions indicate sign changes. The dimensionless geometrical scale factor $c_l(r_0/a,\theta_0)$ (obtained in the Appendix) indicates how strongly the lth-order moment couples to the pick-up loop flux. As long as flux measurements are not to be compared among different pick-up loops, the proportionality constants r_0 and c_l may be absorbed by the field coefficients A_{lm} for convenience.

As the value of l increases, the sensitivity c_l of a pick-up loop to the lth-order moment decreases significantly. Fortunately, this allows the field model to be truncated at finite order. To simplify matters further, c_l is zero for all even values of l for a planar pick-up loop ($\theta_0 = \pi/2$). This is also true of configurations comprised of loop pairs that are parallel and equally spaced from the center of the rotor, such as the Helmholtz configuration. A loop pair connected in series has the effective proportionality constant $c_l = c(\theta_0) + c(\pi - \theta_0)$. For the Helmholtz configuration, the pick-up loops are separated by a distance equal to the loop radius so that $\tan\theta_0 = 2$. For this case, c_3 is also zero, rendering the pick-up loop insensitive to the second-, third-, and fourth-order components of the expansion. In this case, the largest contribution to the measured flux comes from the $l = 1$ or dipole component of the trapped flux.

Figure 8 shows the rotor now oriented with respect to a laboratory (pick-up loop) reference frame. At this point, the rotor z axis has been chosen to coincide with the instantaneous spin axis, and the x axis is aligned with the perpendicular component of the magnetic dipole vector. In this figure, the instantaneous coordinates of the gyroscope spin axis are given by (θ_j,ϕ_j) for the jth pick-up loop axis, and the rotor angle of rotation about the spin axis is given by ωt. Accordingly, with r_0 and c_l absorbed by the field coefficients, the measured flux for the y (smallest) pick-up loop from Eq. (5) is

$$\Phi_M(t) = \sum_{l\,\text{odd}} \sum_{m=-l}^{l} A_{lm} Y_{lm}(-\theta_y, -\omega t) \qquad (6)$$

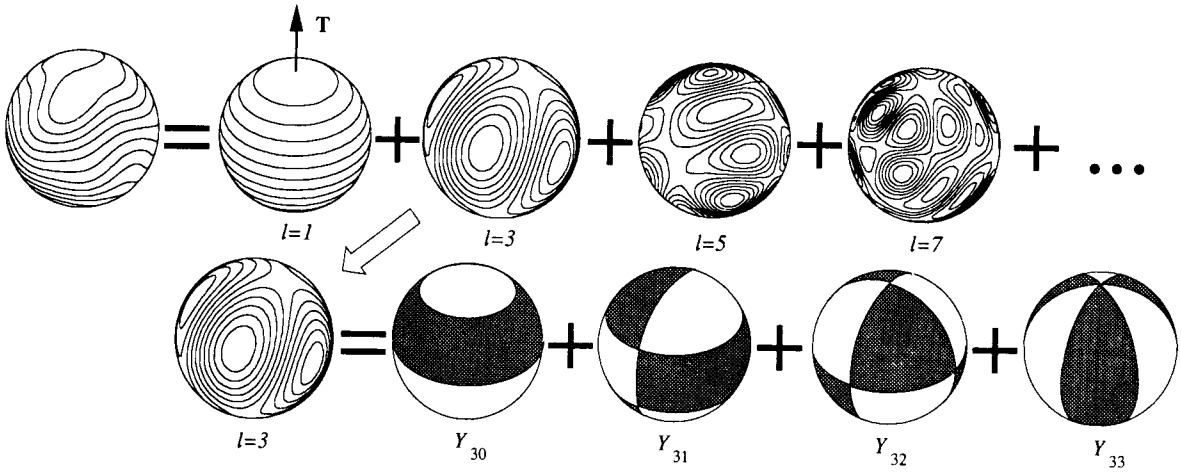

Fig. 7 Topographical interpretation of pick-up loop measurements [Eq. (5)].

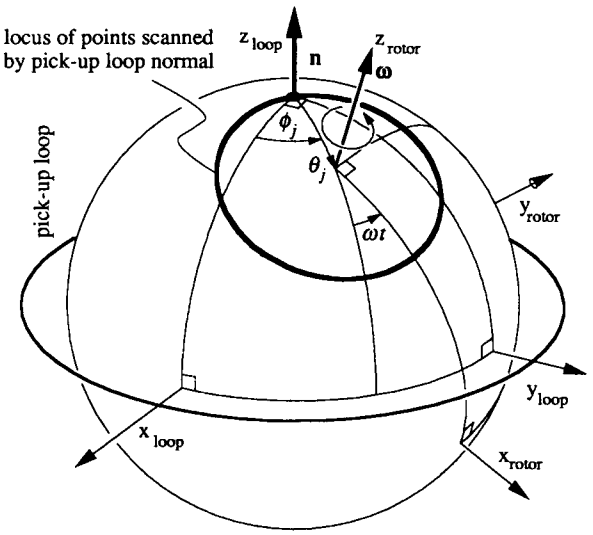

Fig. 8 Locus of points scanned on rotor surface.

As can be seen from the figure, the pick-up loop normal will scan across a circle on the surface of the rotor and yield a signal that is periodic in ω. Based on the decomposition $Y_{lm}(-\theta_y, -\omega t) = Y_{lm}(-\theta_y, 0)e^{-im\omega t}$ (for $m \geq 0$), the Fourier coefficients of Eq. (1) are (for $m \geq 0$)

$$\Phi_m^* = \sum_{l \text{ odd}, \geq m} A_{lm} Y_{lm}(-\theta_y, 0) \tag{7}$$

This observation equation relates the Fourier components of the measurement spectrum to the spherical harmonic coefficients. Output at a given harmonic m of the fundamental frequency ω is simply a linear combination of the spherical harmonics of the same degree, m.

Trapped Flux Model in Context of Rotor Dynamics

Three different time scales are present in the output of the pick-up loops. In general, the spin rate ω is much faster than either the polhode or precession rates. Note that, for the range of inertia difference ratios $k = \Delta I/I \approx 10^{-4}$, the angular momentum and spin axes are aligned within an angle $k/2$ rad (or less), which may be considered negligible for this treatment.

For the prototype gyroscopes undergoing ground tests, the dominant external torque arises from the suspension system acting on the rotor asphericity. The fundamental component of suspension torque is the mass unbalance. Earth rotation also produces an effective precession since the laboratory is not a true inertial reference frame. Figure 9 shows examples of the rotor motion in both the laboratory and body reference frames. Under the influence of gravity and Earth rotation, the spin axis traces out the path shown in the laboratory frame, allowing the angle θ_y between the spin and laboratory y axes to vary considerably over the precession cycle. The smaller scale cusps shown in the inset of Fig. 9a are caused by polhode motion modulating the rotor asphericity torque.

In the rotor body frame, the spin axis traces out a polhode. Note in Figs. 9c and 9d that, as the rotor polhodes, the compo-

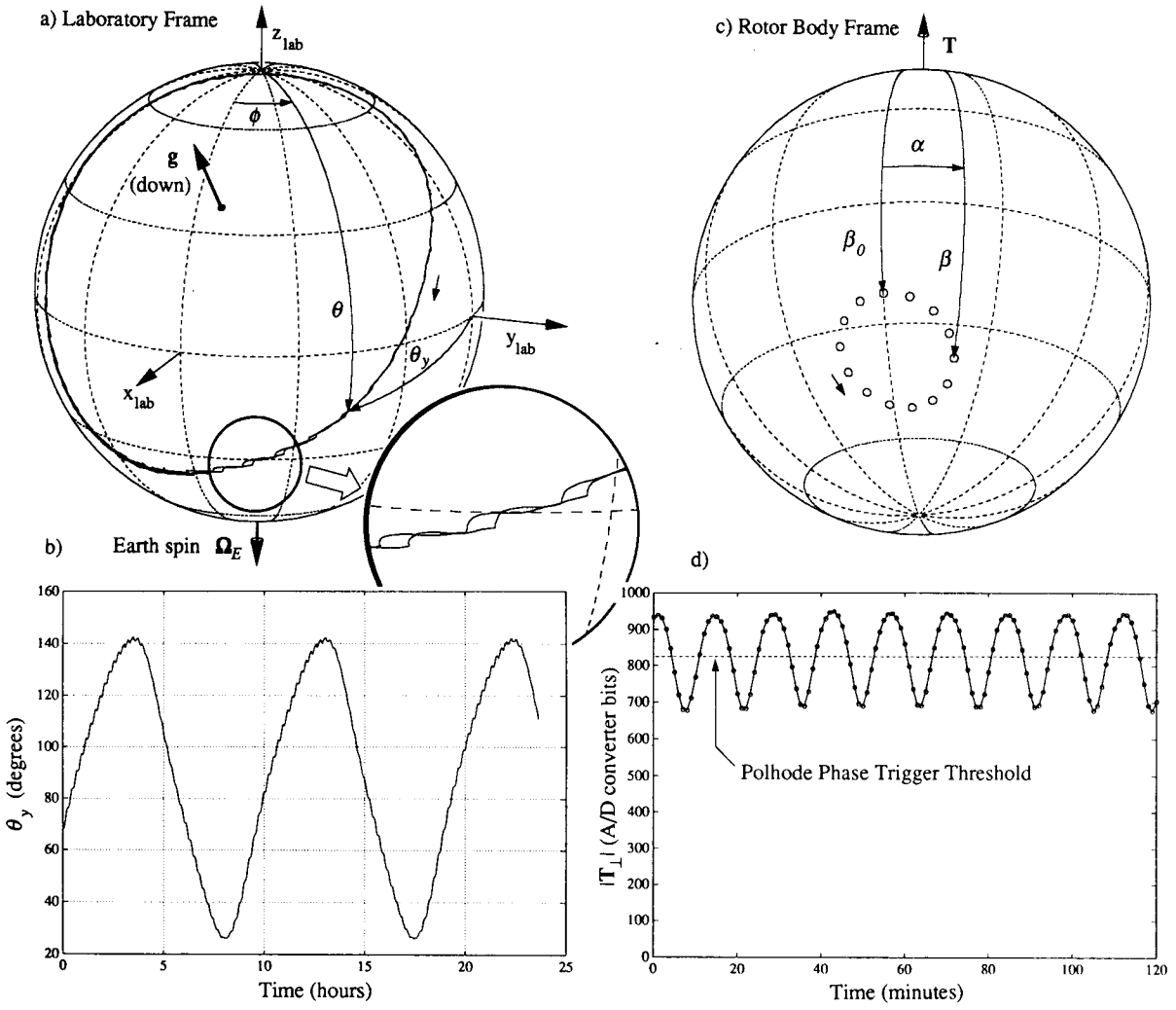

Fig. 9 Precession and polhoding: spin axis motion in two reference frames for a spin rate of 11 Hz: a) laboratory frame; b) precession signature; c) rotor body frame; d) polhode signature.

nent of the trapped flux dipole moment perpendicular to the spin vector changes.

In the experimental apparatus, the Helmholtz configuration in conjunction with the large loop radius attenuates the higher-order moments of the rotor magnetic field. What remains is the dipole component, producing an output that is sinusoidal to within 2%. Reference 4 shows how the orientation (θ,ϕ) of the gyroscope spin axis in the laboratory frame may be determined from the sinusoidal output of the two outer pick-up loops. Furthermore, this same output may also be used to solve for the component of the dipole moment perpendicular to the spin axis shown in Fig. 9d.

The finer detail of the magnetic field is measured with the y axis pick-up loop, which is located close to the surface of the rotor. Output from this loop is used to estimate the trapped flux shape and reconstruct the polhode motion of the rotor. Although many filtering schemes are applicable to estimation

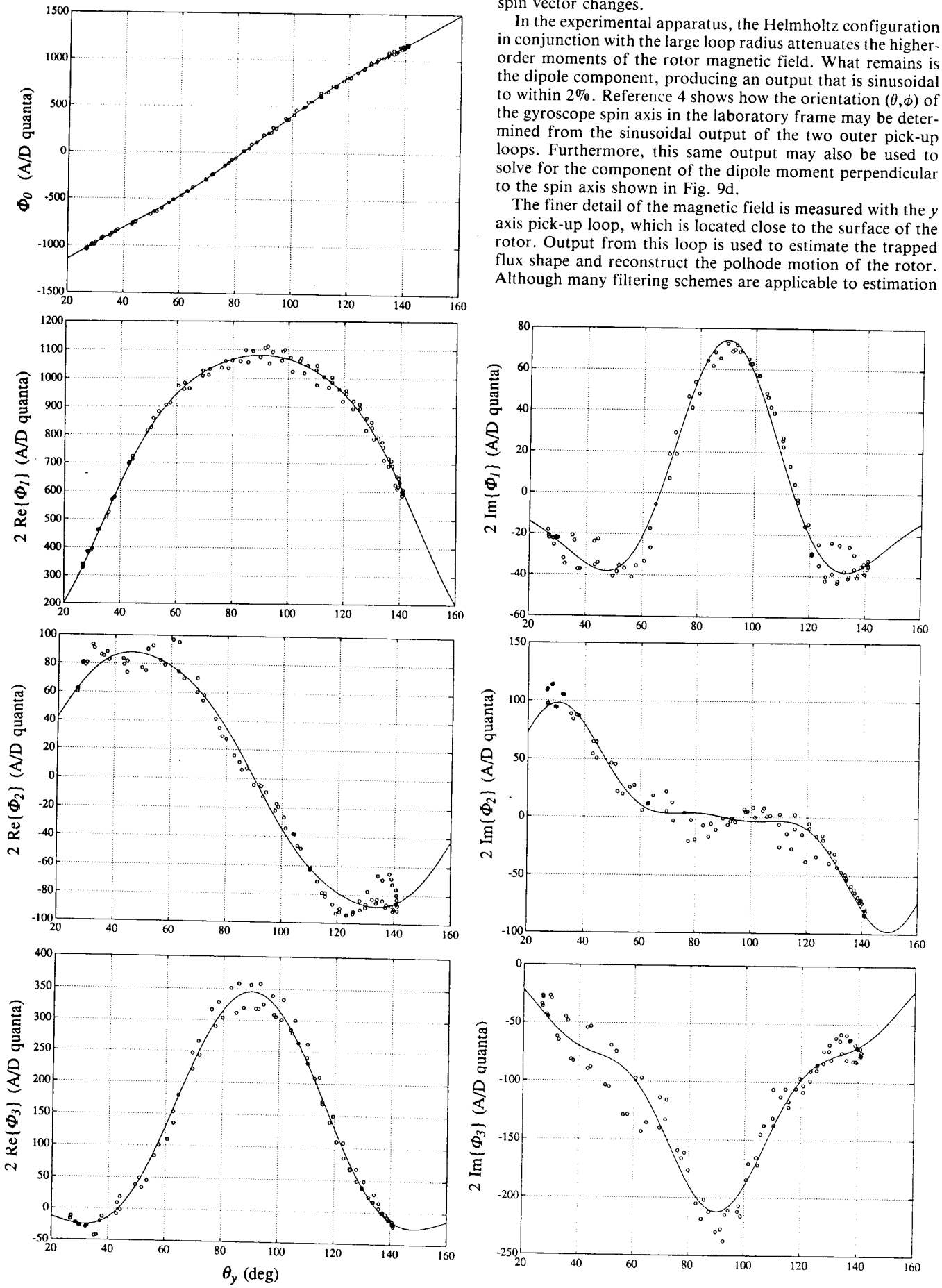

Fig. 10 Fourier components of inner pick-up loop signal.

of the polhode motion from pick-up loop measurements, only one such technique is presented here.

Bootstrapping the Estimation

To build a model of the higher-order magnetic field from data coming from a single pick-up loop, it is assumed that the rotor spin axis traces out the same polhode path over the time period of interest. Although this is usually valid for higher spin rates where gyroscopic torques dominate, external torques overcome the polhode motion at lower spin rates.

The problem of determining the coefficients of the trapped flux model is greatly simplified by considering data only when the spin axis lies at a single point in the polhode cycle. From the perpendicular component of the trapped flux determined from the outer pick-up loops shown in Fig. 9d, the relative phase of the polhode cycle may be determined by choosing the rising time of the transition across a threshold as a reference. Since two adjacent bursts of data may straddle the threshold crossing, interpolation is employed. If all of the intervening data between transitions are thrown out, the polhode motion is effectively eliminated from the data since, according to the assumption, the spin axis has returned to precisely the same position it had in the previous polhode cycle. In the same manner that a strobe light appears to halt periodic motion, "snapshots" of the data are taken at exactly the right time in the polhode cycle so that the spin axis appears to stay fixed in the body frame.

Building up an Estimate of the Rotor Field

With the polhode motion effectively eliminated for the time being, the precession of the gyroscope varies the angle θ_y between the small pick-up loop and the spin axis (as shown in Fig. 9b). Considering the spin axis as the north pole of the rotor, the pick-up loop normal scans different lines of latitude as θ_y evolves. For favorable ranges of θ_y over a precession cycle, almost all of the rotor surface area can be scanned.

The outer pick-up loops provide the phase reference based on the dipole moment, defining a longitude reference for the small pick-up loop signal. The A_{lm} coefficients in Eq. (7) may be determined through a least-squares fit. Figure 10 shows the Fourier coefficients (through the third harmonic) of the small pick-up loop signal plotted against θ_y. The experimental data points are indicated by circles, and the solid lines are the best-fit curves for a seventh-order model of the trapped flux field. The symmetry about $\theta_y = 90$ deg is a manifestation of the planar pick-up loop ($c_{l\,\text{even}} = 0$).

Estimating Spin Axis Motion

The polhode motion is determined by comparing the estimated fields built up from different points in the polhode cycle. One may determine the times at which the spin axis passes through points in the polhode cycle by interpolating between times of threshold crossings of $|\boldsymbol{T}_\perp|$ in Fig. 9d. By rebuilding the trapped flux model at a different point in the polhode cycle, the resulting magnetic field should differ from the reference by a rotation only. The spin axis path is reconstructed by determining the angles of rotation resulting in the best fit of the two fields.

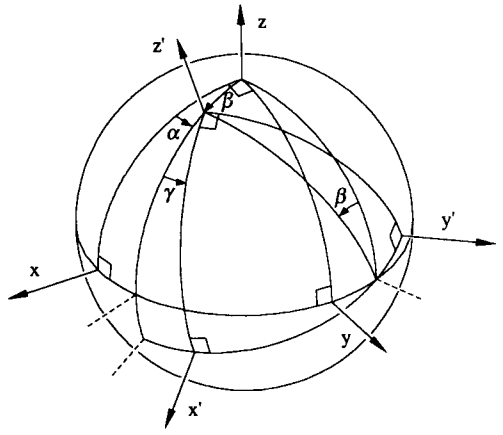

Fig. 11 Angle definitions for coordinate transformations.

Spherical harmonics may be expressed in terms of harmonics in a rotated reference frame based on D transformation matrices.[5] For the rotated reference frame defined by the 3-2-3 Euler angles (α,β,γ) shown in Fig. 11, the spherical harmonics in the primed frame may be expressed as

$$Y_{lm'}(\theta',\phi') = \sum_{m=-l}^{l} D^{l}_{mm'}(\alpha,\beta,\gamma)\, Y_{lm}(\theta,\phi) \tag{8}$$

A spherical harmonic function of a given order l and degree m is a linear combination of the rotated spherical harmonics of the same order. Rotation of the spherical harmonic functions is equivalent to a (reverse) rotation of the coefficients:

$$A'_{lm'} = \sum_{m=-l}^{l} D^{l}_{m'm}(-\gamma,-\beta,-\alpha) A_{lm} \tag{9}$$

Through Eqs. (4), the angle β between the spin axis and the trapped flux vector may be calculated since $\cos\beta = T_z/|\boldsymbol{T}|$. By Eq. (9), a set of field coefficients may be rotated by angle β to position the trapped flux dipole vector at the north pole of the rotor. The rotated reference coefficients A^{ref}_{lm} define the rotor fixed frame. Coefficient sets from other points in the polhode cycle also can be rotated to position the trapped flux vector at the north pole. These coefficient sets should differ from the reference only by a polar rotation α. Note that any order moment of the field other than the axially symmetric dipole may be used to determine this angle. For simplicity, the $l = 3$ component of the field is chosen since it has the fewest coefficients.

The polar rotation angle α is determined through a nonlinear least-squares fit that minimizes the integral over the entire rotor surface of the square of the measured potential error. Since Eq. (9) reduces to $A'_{lm} = e^{im\alpha} A_{lm}$, this minimum may be shown to be equivalent to finding the value of α that minimizes the norm

$$\left\| \begin{bmatrix} A'_{31} \\ A'_{32} \\ A'_{33} \end{bmatrix} - \begin{bmatrix} e^{i\alpha} A^{\text{ref}}_{31} \\ e^{i2\alpha} A^{\text{ref}}_{32} \\ e^{i3\alpha} A^{\text{ref}}_{33} \end{bmatrix} \right\|_2 \tag{10}$$

Results

The methodology just described was applied to measurements taken with the prototype Gravity Probe B rotor 87R11c. This rotor, spinning at 11 Hz, exhibited a polhode period of 14 min. Figures 1, 7, 9, and 10 all depict results from a single set of measurements taken over a 24-h interval. Figure 7 shows the estimated rotor magnetic field shape, and Fig. 1 shows the estimated polhode and the inferred principal axis locations.

Sources of Error

The two dominant error sources in estimating the reference magnetic field are thought to be the assumption that the spin axis follows the same polhode path independent of orientation in the laboratory and imperfections in the geometry of the pick-up loops. Note that the data plotted in Fig. 10 exhibit a systematic component (hysteresis). Other sources of error thought to be less significant are eddy currents generated by the magnetic fields and readout noise. In the gyroscope design, the use of metal near the gyroscope has been kept to a minimum.

Applications of Tracking Technique

Knowledge of the polhode motion is useful for analyzing physical parameters of the gyroscope. The polhode size, eccen-

tricity, orientation, and period directly yield the rotor inertia tensor. Furthermore, the shape of the rotor surface may be estimated relative to the principal inertia axes by correlating precession with polhode motion.[3] Rotor asphericity influences the gyroscope motion since forces and moments applied by the electrostatic suspension system are dependent on the spacing between the electrodes and the rotor surface. Figure 9a shows cusps in the spin axis path due to the polhode motion modulating these suspension torques. Last, polhode tracking offers considerable insight into the magnetic environment of the gyroscope. The sizes of the field model coefficients reflect the strength and homogeneity of the ambient magnetic field before the rotor becomes superconducting (usually completed before the rotor is initially levitated). The long-term stability of the trapped flux may also be studied since the trapped flux may be referenced with respect to the principal axes of inertia (which are assumed to be fixed in the rotor body frame).

Conclusion

A method is presented for estimating the polhode motion of a cryogenic, free-rotor gyroscope using measurements of trapped magnetic flux. The magnetic field of the superconducting rotor is modeled as a series expansion in spherical harmonics. The dipole moment of the rotor provides one coordinate of the spin axis location in the body frame. The second coordinate is provided by using higher-order moments of the rotor magnetic field. Thus, the spin axis location in the rotor body frame is unambiguously defined.

Appendix: Derivation of Pick-Up Loop Flux

The magnetic flux enclosed by an axially symmetric pick-up loop given in Eq. (5) may be derived by integrating the radial component of the magnetic field B_r over the solid angle enclosed by the pick-up loop, which is shown in Fig. 6. Making use of Eq. (2), the radial component of the rotor magnetic field is

$$B_r(a) = -\left.\frac{\partial V_M}{\partial r}\right|_{r=a} = \frac{r_0}{a^2}\sum_{l=1}^{\infty}(l+1)\left(\frac{r_0}{a}\right)^l \sum_{m=-l}^{l} A_{lm}\,Y_{lm}(\theta_R,\phi_R) \tag{A1}$$

Adapting Eq. (8) for the pick-up loop positioned at coordinates (β,α),

$$Y_{lm}(\theta_R,\phi_R) = \sum_{n=-l}^{l} D^l_{nm}(0,-\beta,-\alpha)\,Y(\theta_L,\phi_L) \tag{A2}$$

The magnetic flux Φ_m through the pick-up loop is

$$\Phi_m(\beta,\alpha) = \int_0^{\theta_0}\int_0^{2\pi} B_r(a)a^2 \sin\theta_L \, d\phi_L \, d\theta_L \tag{A3}$$

Substituting Eqs. (A1) and (A2) into Eq. (A3), it is seen that the axial integral vanishes for $n \neq 0$ because the pick-up loop is axially symmetric:

$$\Phi_m(\beta,\alpha) = 2\pi r_0 \sum_{l=1}^{\infty}(l+1)\left(\frac{r_0}{a}\right)^l \int_0^{\theta_0} Y_{l0}(\theta_L,\phi_L)\sin\theta_L \, d\theta_L \times \sum_{m=-l}^{l} A_{lm}D^l_{0m}(0,-\beta,-\alpha) \tag{A4}$$

In this case where $n = 0$, it can be shown from Eq. (A2) and the spherical harmonic addition theorem that

$$D^l_{0m}(0,-\beta,-\alpha) = \sqrt{\frac{4\pi}{2l+1}}\,Y_{lm}(\beta,\alpha) \tag{A5}$$

Substitution of Eq. (A5) into Eq. (A4) yields Eq. (5), where the dimensionless coupling coefficients c_l are given by

$$c_l\left(\frac{r_0}{a},\theta_0\right) = 2\pi(l+1)\sqrt{\frac{4\pi}{2l+1}}\left(\frac{r_0}{a}\right)^l \int_0^{\theta_0} Y_{l0}(\theta_L,0)\sin\theta_L \, d\theta_L \tag{A6}$$

Acknowledgment

This research was performed under NASA Contract NAS8-36125.

References

[1]Turneaure, J. P., et al., "The Gravity Probe B Relativity Gyroscope Experiment: Development of the Prototype Flight Instrument," *Advances in Space Research*, Vol. 9, No. 9, 1989, pp. 29–38.

[2]Keiser, G. M., and Cabrera, B., "Trapped Flux Readout for an Electrostatically Supported Superconducting Gyroscope," *Proceedings of the National Aerospace Meeting*, Institute of Navigation, Washington, DC, March 1982, pp. 75–79.

[3]Feteih, S., Keiser, G. M., Breakwell, J. V., and Xiao, Y., "Results of Dynamic Testing of GP-B Spherical Gyroscopes," *Proceedings of the Guidance, Navigation, and Control Conference*, AIAA Paper 89-3439, AIAA, Washington, DC, 1989, pp. 123–140.

[4]Feteih, S., Keiser, G. M., and Breakwell, J. V., "Mass Unbalance Analysis for GP-B Rotors," *Proceedings of the Guidance, Navigation, and Control Conference*, AIAA Paper 88-4178, AIAA, Washington, DC, 1988, pp. 1041–1052.

[5]Rose, M. E., *Elementary Theory of Angular Momentum*, Wiley, New York, 1957, Chap. 4.